Structural basis of mouse cytomegalovirus m152/gp40 interaction with RAE1γ reveals a paradigm for MHC/MHC interaction in immune evasion

Rui Wang[a], Kannan Natarajan[a], Maria Jamela R. Revilleza[a], Lisa F. Boyd[a], Li Zhi[a,1], Huaying Zhao[b], Howard Robinson[c], and David H. Margulies[a,2]

[a]Molecular Biology Section, Laboratory of Immunology, National Institute of Allergy and Infectious Diseases, National Institutes of Health, Bethesda, MD 20892; [b]Dynamics of Macromolecular Assembly Section, Laboratory of Cellular Imaging and Macromolecular Biophysics, National Institute of Biomolecular Imaging and Bioengineering, National Institutes of Health, Bethesda, MD 20892; and [c]National Synchrotron Light Source, Brookhaven National Laboratories, Upton, NY 11973

Edited by K. Christopher Garcia, Stanford University, Stanford, CA, and approved October 24, 2012 (received for review August 17, 2012)

Natural killer (NK) cells are activated by engagement of the NKG2D receptor with ligands on target cells stressed by infection or tumorigenesis. Several human and rodent cytomegalovirus (CMV) immunoevasins down-regulate surface expression of NKG2D ligands. The mouse CMV MHC class I (MHC-I)–like m152/gp40 glycoprotein down-regulates retinoic acid early inducible-1 (RAE1) NKG2D ligands as well as host MHC-I. Here we describe the crystal structure of an m152/RAE1γ complex and confirm the intermolecular contacts by mutagenesis. m152 interacts in a pincer-like manner with two sites on the α1 and α2 helices of RAE1 reminiscent of the NKG2D interaction with RAE1. This structure of an MHC-I–like immunoevasin/MHC-I–like ligand complex explains the binding specificity of m152 for RAE1 and allows modeling of the interaction of m152 with classical MHC-I and of related viral immunoevasins.

immune recognition | virus evasion | X-ray diffraction

Cytomegaloviruses (CMV), members of the β-herpesvirus family, pathogenic in immunosuppressed or immunodeficient hosts (1), may lie dormant for many years but can cause considerable morbidity and mortality with neonatal or HIV infection or during organ transplantation (2). The large size of the CMV dsDNA genomes (as large as 250 kb), allows these viruses to dedicate many genes to viral fitness; a number of these genes thwart the host inflammatory, innate, and adaptive immune responses. Human and mouse studies emphasize the importance of natural killer (NK) and $CD8^+$ T cells in the antiviral response, underscoring the complementary roles of innate and adaptive immunity. Of particular importance to NK-mediated immunity is NKG2D, a C-type lectin-like homodimeric glycoprotein that mediates NK cell activation on ligation by host molecules expressed at the cell surface as a result of cellular or genotoxic stress (3, 4). Human NKG2D ligands include MICA, MICB, and members of the ULBP family (4, 5), and studies suggest a complex relationship between the expression of NKG2D ligands on tumor cells, the effectiveness of immunosurveillance, and clinical prognosis (6, 7). Murine NKG2D recognizes RAE1 family members (RAE1α–ε), H60 (H60a–c), and the murine UL16-binding protein-like transcript 1 (MULT1) (8–10). Remarkably, these NKG2D ligands are related to MHC class I (MHC-I)–like molecules (11, 12), and several are targets of MHC-I–like immunoevasins (3). In particular, mouse CMV (MCMV) m152/gp40 (hereafter referred to as "m152") has a dual role, downregulating cell-surface expression of RAE1 family members [but not MULT1 or H60 (13), the targets of MCMV proteins m145 and m155, respectively (14, 15)] as well as host MHC-I molecules (16–19). A virus-encoded Fc receptor, m138, also controls MULT1, H60 (3), and RAE1ε (20). In vivo, MCMV deletions lacking m145, m152, m155, or m138 are defective in viral control of surface expression of MULT1, RAE1, and H60.

To explore the mechanism by which MCMV MHC-I–like immunoevasins interact with and down-regulate their respective NKG2D ligands, we examined the binding of the MCMV m152 glycoprotein to its RAE1 ligands. Our previous studies investigated the quantitative interaction of m152 with different RAE1 isoforms (21). Here we report the X-ray structure of the complex of m152 with RAE1γ, the confirmation of the intermolecular contacts observed in the crystal structure by site-directed mutagenesis and in vitro binding assays, a comparison of the binding of m152 to RAE1 and of NKG2D to RAE1, and the functional effects of selected RAE1 mutants in their susceptibility to down-regulation by m152. These results also provide a structural basis for modeling the interaction of m152 with MHC-I molecules, offer a foundation for understanding the interactions of the related m145 and m155 molecules with their respective MULT1 and H60 ligands, provide insight into the mechanisms that contribute to the evolution of the m145 family of MCMV immunoevasins, and allow speculation about the structural basis of the interaction of the HCMV immunoevasin UL142 with its MICA ligand.

Results

Overall Structure of the m152/RAE1γ Complex. m152 binds the γ isoform of RAE1 with the greatest affinity compared to the other isoforms, permitting the purification of m152/RAE1γ complexes. We obtained crystals of the complex diffracting to 2.45 Å, and molecular replacement solutions were obtained using the previously determined structures of MCMV m153 (22) and RAE1β (11) (see *Materials and Methods* for details). Structural refinement proceeded well (Table S1), and continuous electron density was observed throughout the map, with small breaks in loops as noted in *Materials and Methods*. The asymmetric unit consists of two heterodimeric complexes (Fig. 1*A*), but, based on our previously published analysis of the stoichiometry of the m152/RAE1 interaction, the 1:1 heterodimer is the biologically significant structure (21). Because the two heterodimers are essentially identical (rmsd of 0.194 Å for 356 superposed Cα), we have limited our description of the complex and its components to the first heterodimer in the asymmetric unit.

Author contributions: R.W., K.N., and D.H.M. designed research; R.W., K.N., M.J.R.R., L.F.B., L.Z., H.R., and D.H.M. performed research; R.W., K.N., L.F.B., H.Z., and D.H.M. analyzed data; and R.W., K.N., and D.H.M. wrote the paper.

The authors declare no conflict of interest.

This article is a PNAS Direct Submission.

Data deposition: The coordinates and structure factors have been deposited with the Protein Data Bank, www.pdb.org (PDB ID code 4G59).

[1]Present address: Division of Hematology, Office of Blood Research and Review, Center for Biologics Evaluation and Research, Food and Drug Administration, Bethesda, MD, 20892.

[2]To whom correspondence should be addressed. E-mail: dhm@nih.gov.

See Author Summary on page 20786 (volume 109, number 51).

This article contains supporting information online at www.pnas.org/lookup/suppl/doi:10.1073/pnas.1214088109/-/DCSupplemental.

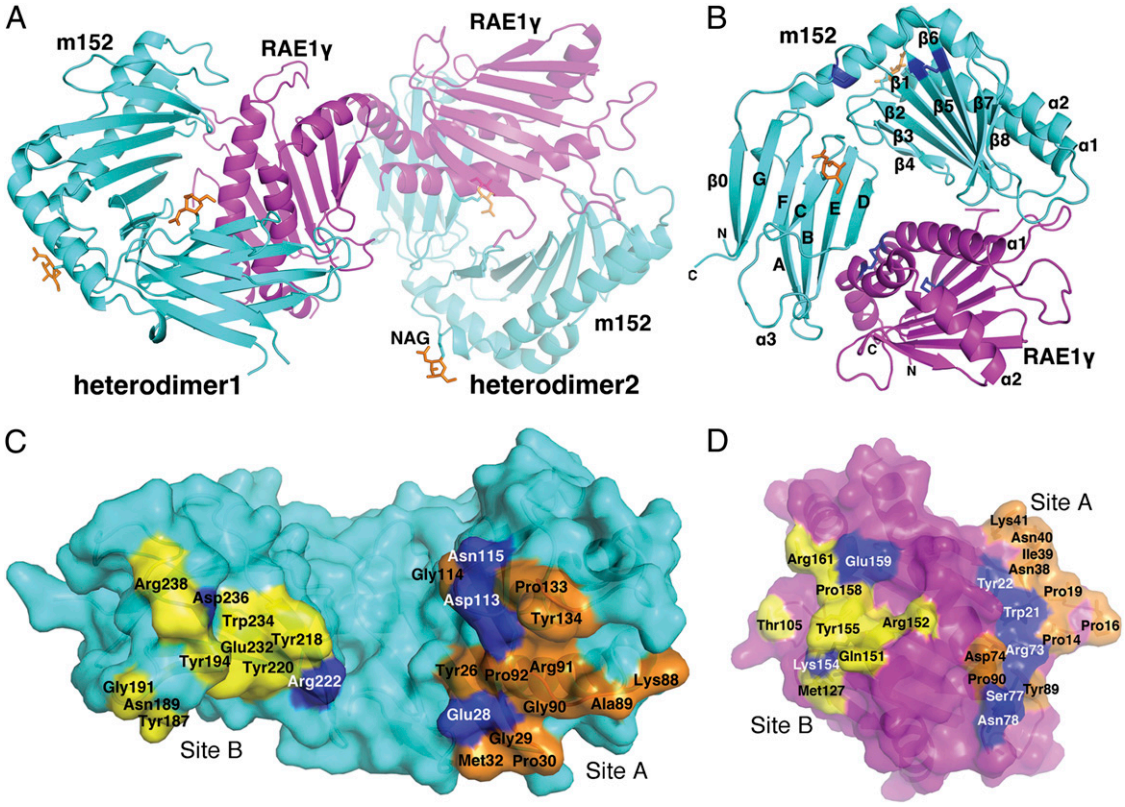

Fig. 1. Structure of the m152/RAE1γ complex. (*A*) The heterodimeric structure of m152 with RAE1γ complex is shown in a ribbon model. m152 is shown in cyan and RAE1γ in magenta in heterodimers 1 and 2. Heterodimer 2 was 50% transparency. Glycosylated Asn of m152 are shown as ball-and-stick models and are colored orange. (*B*) Ribbon drawing of m152/RAE1γ 1. Disulfide bonds are blue. (*C*) Residues of m152 that contact RAE1γ are illustrated in a surface model. Residues at Site A are orange, residues at Site B are yellow, and all hydrogen bond residues are blue. (*D*) Residues of RAE1γ that contact m152. The colors of contact residues are the same as m152 in *C*.

The overall fold of m152 resembles an MHC-I α1α2 platform domain (pd) joined to an Ig-like α3 domain. Scanning the Dali database (23) gives high-scoring hits not only with other MCMV-encoded MHC-Iv (viral-encoded MHC-I) proteins, m153 and m157, but also with MHC-I fold proteins such as RAE1β, FcRn (the neonatal Fc receptor), HFE, and HLA-A2 (Z scores of 24.6, 17.0, 12.6, 11.9, 11.9, and 11.9 respectively). Consistent with expression studies indicating that m152 has no requirement for either a β2m subunit or peptide (19, 22), we observe no unaccounted electron density. The m152 α1α2 domain is composed of one long α1 helix (residues 61–86, with a break between 64 and 65) and one discontinuous α2 helix (residues 139–182, with breaks at residues 147, 158, and 178) in an antiparallel orientation (Fig. 1*B* and Fig. S1). These two helices are supported by a platform of eight antiparallel β-strands, the first four of which derive from the α1 domain and the remainder from α2. The two α-helices of m152 lie closer to each other than in classical MHC-I molecules, eliminating space for a peptide or other nonpeptidic ligand. A novel disulfide bridge also seen in m153 (22) between Cys16 and Cys170 connects N-terminal residues with the α2 helix and rigidifies the relationship between the α1α2 pd and α3. The α2 domain is stabilized by a disulfide bond (Cys99 to Cys106) that joins strands β5 and β6; this bond is conserved among most MHC-Iv molecules but is missing in m157 (19).

Because of the substitution of Cys248 by Phe (Fig. S1) the α3 domain lacks the intradomain disulfide joining Cys197 to Cys248 found in most other MHC-Iv proteins. This domain is characterized by a novel eight-stranded variation on the seven-stranded C1-type Ig-fold (24), adding a β0 strand from the amino terminus to the three-stranded sheet (Fig. 1*B* and Fig. S1). This β0 strand aligns with strand G, and a second β-sheet derives from strands A, B, E, and D (Fig. 1*B* and Fig. S1). The N-terminal regions of other known structures of MCMV-encoded MHC-Iv proteins vary: m153 has a short β-strand at the N-terminal region (22), m157 has an α0 helix at its N terminus (25), and m144 lacks an N-terminal extension (26). The m152 glycoprotein is expected to have asparaginyl-carbohydrate moieties at positions 61, 208, and 241. We observed electron density for two single *N*-acetyl glucosamine residues at Asn61 (located at the N terminus of the α1 helix) and at Asn208 (on the C-strand beneath the pd) and have modeled them in the structure (Fig. 1*A* and *B*). These positions are distant from the m152/RAE1γ interface and are not expected to affect that interaction.

Comparison of m152 and RAE1γ with Classical MHC Class I and MHC Class I Homologs. In addition to the strong structural similarities of m152 with m153 and m157, the m152 α1α2 pd is remarkably similar in structure to its ligands RAE1β and RAE1γ (for β, 4% identical in amino acid sequence, rmsd 3.2 Å, Z score 12.6; for γ, 5% identical, rmsd 3.0 Å, Z score 11.7). Although similar, the topology of m152 deviates from that of classical MHC-I molecules. Superposition of the MHC-I molecule H2-D^d heavy chain with m152 gives an rmsd of 5.71 Å. Comparing m152 with MHC-Ib and MHC-Iv molecules, such as CD1a, MICA, m144, m153, m157, UL18, and tanapox 2L, we observe that m152 is most similar to the MHC-Iv molecules and among them is closest to m153 (Fig. 2*A*). m153 is a noncovalent homodimer (22), whereas the m152/RAE1γ crystal structure shows that m152 binds RAE1 as a monomer. Additional features distinguish m152 from other MHC-Iv molecules. In Fig. 2*B*, we compare the α1α2 domain of m152 with that of RAE1, m153, m144, m157, H2-D^d, CD1a,

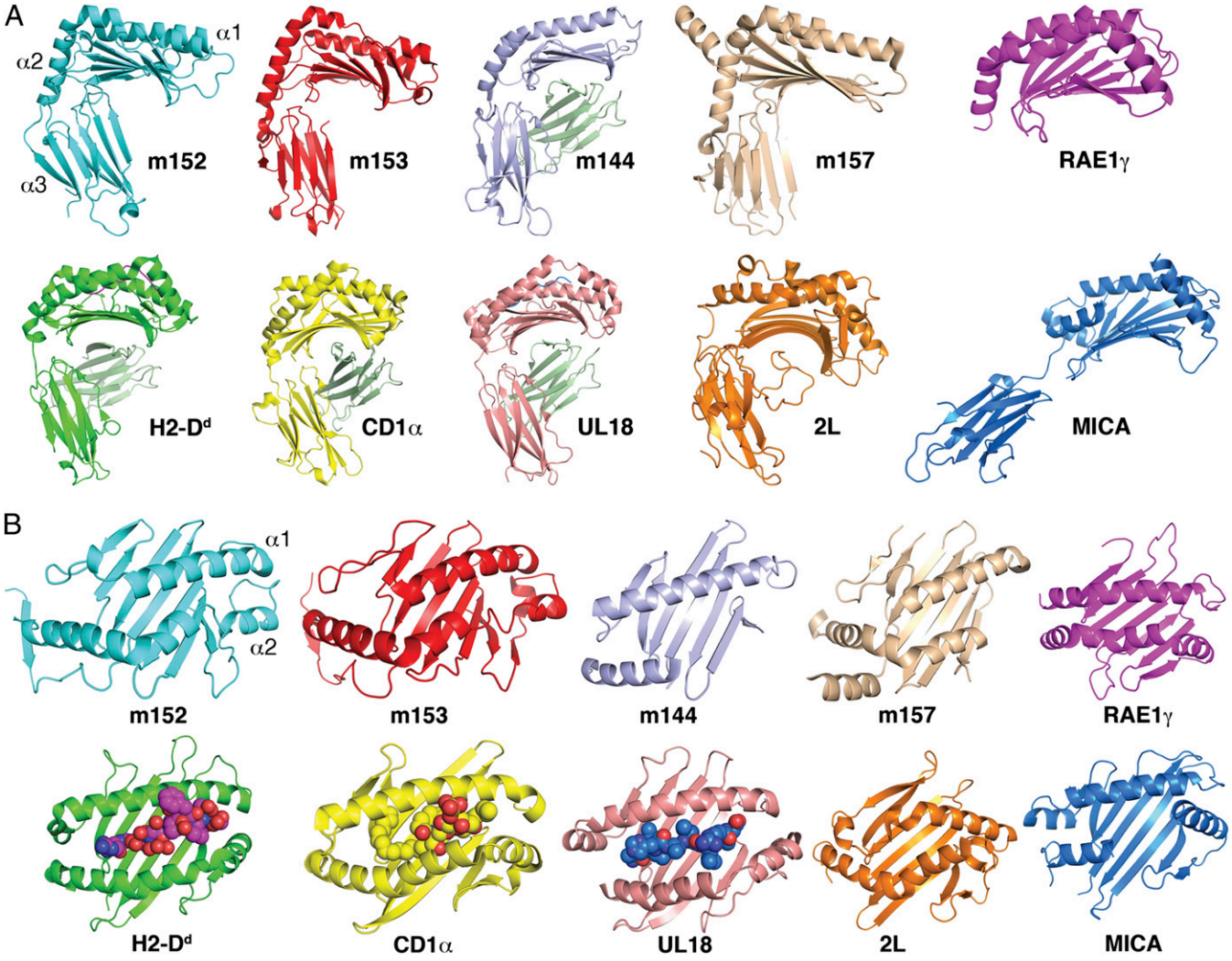

Fig. 2. Comparison of structural features of m152 and other MHC-I, MHC-Ib, and MHC-Iv molecules illustrated as ribbon diagrams and in the same orientation. (*A*) The structures of m153 (PDB ID 2O5N), m144 (PDB ID 1U58), m157 (PDB ID 2NYK), RAE1γ, H-2-D^d (PDB ID 3ECB), CD1a (PDB ID 1ONQ), UL18 (PDB ID 3D2U), 2L (PDB ID 3IT8), and MICA (PDB ID 1B3J) were each superposed on m152. (*B*) The α1α2 pd of m152 was superposed on m153, m144, m157, RAE1γ, H-2-D^d, CD1a, UL18, 2L, and MICA.

UL18, MICA, and the tanapox 2L protein. The hinge angle between the α1α2 unit and the α3 domain of m152 is 68°, similar to those of m153 (76°), H2-D^d (68°), and CD1a (71°) but less than the hinge of two other MHC-Iv molecules, m157 (81°) and m144 (99°), and much less than that of MICA (116°). The maximal distance between the α1 and α2 helices across the groove of m152 is 8.2 Å, similar to that of m153 (8.1 Å) and m157 (8.4 Å), in contrast with MHC-I proteins that bind either peptide or glycolipid ligands and have much wider grooves [e.g., H2-D^d (16.3 Å), Ul18 (14.3 Å), and CD1a (12.9 Å)].

RAE1γ is 88% identical to RAE1β in amino acid sequence (Fig. S2*A*), and the structures are almost identical as well, with clear structural similarity to MHC-I molecules. Like RAE1β, RAE1γ lacks a peptide-binding groove and preserves a long α1 helix and a discontinuous α2 helix arranged above a seven-stranded antiparallel β-sheet (Fig. 2 and Fig. S2). The rmsd for the superposition of RAE1γ and RAE1β is 0.645 over 132 Cα. Of the five predicted N-linked glycosylation sites of RAE1γ, four—Asn8, Asn40, Asn53, and Asn113—are conserved among all the isoforms, and Asn126 is found in all but RAE1δ (Fig. S2*A*). None of these impinge on either the m152/RAE1γ or on the NKG2D/RAE1β interface (11).

Interface Between m152 and RAE1γ. m152 interacts with RAE1γ as a pair of pincers with two surfaces, one derived from the floor of its α1α2 pd (site A), and a second from its α3 domain (site B) (Fig. 1*C*). These two surfaces bestride the saddle-like antiparallel α1 and α2 helices of RAE1γ (Fig. 1*D*), leaving a small central channel accessible to solvent. The total solvent-accessible surface area buried at the m152/RAE1γ interface is about 2,600 Å^2 (2,640 Å^2 for heterodimer 1, 2,530 Å^2 for heterodimer 2), an area larger than that of the typical MHC-I/TCR recognition interface (1,700–1,800 Å^2) (27) and also greater than the interface of mNKG2D/RAE1β (1,700 Å^2) (11), hNKG2D/MICA (2,200 Å^2) (28), and UL16/MICB (2,194 Å^2) (29). Unlike NKG2D, which forms a homodimer to bind its ligands, m152 binds monomerically to RAE1. The interface shape complementarity (Sc) value is 0.68, slightly greater than that of the mNKG2D/RAE1β complex (Sc = 0.63) (11) and about the same as that of TCR/MHC interfaces (~0.65–0.7) (27).

At site A, the m152 N-terminal region (Tyr26 to Met32, Lys88 to Pro92) interacts with RAE1γ N-terminal loops (Pro14 to Tyr22 and Asn38 to Lys41) (Fig. 1 C and 1D, Fig. 3*A* and Tables S2 and S3). Glu28 of m152 forms hydrogen bonds to Trp21 and Tyr22 of RAE1γ. In addition, Asp113 and Asn115 of m152 hy-

drogen bond to Arg73, Ser77, and Asn78 of the α1 helix of RAE1γ (Fig. 3*B* and Tables S2 and S3). At site B, residues of the α3 domain of m152 interact with RAE1γ via a surface comprised of strands A, B, E, and D (Figs. 1 *B* and *D* and 3 *C* and *D*). [One residue of m152, Arg222, contacts residues of both site A and B of RAE1γ (Tables S2 and S3).] The mode of interaction of the MHC-I–like molecule m152 with RAE1γ contrasts with the interaction site of T-cell receptor (TCR) with classical MHC-I molecules, where the TCR binding site, composed of the complementarity-determining regions of the TCR Vα and Vβ chain, interacts with the MHC α1 and α2 helices (and bound antigenic peptide). The human NK cell immunoglobulin-like (KIR) NK cell receptors interact primarily with residues of the MHC helices, although interaction with bound peptide is limited (30). The interaction site of m152 with its RAE1γ ligand mimics more closely the region of contact of mouse MHC-I molecules with the C-type lectin-like NK receptors of the Ly49 family, where the interaction is through a broad surface involving the floor of the pd and the α3 domain (31). In contrast, UL16, a monomeric single Ig-like domain, engages the α1α2 pd of MICB through a single surface (29), through contacts to the α2 helix of MICB at a site analogous to site B of the m152/RAE1 interface.

Interface Mutants of RAE1γ Affect Binding of m152. To evaluate further the structural interface between m152 and RAE1γ, we made mutants of RAE1γ. We studied the binding of mutants at 10 positions, five from site A and five from site B (Fig. 4 *A* and *B*, Table 1, and Fig. S3 *A* and *C*). For RAE1γ binding at site A, we examined W21A, N38A, R73A, S77A, S77E, and S77L as single mutants and the double mutants R73A/N78A and S77A/N78A. Compared with the parental RAE1γ, mutants at position 77 had a modest effect ($\Delta\Delta G$ = 0.88–0.96 kcal/mol) and substitutions of W21, N38, and R73 were somewhat greater ($\Delta\Delta G$ = 1.38–1.47 kcal/mol). This result is consistent with the hydrogen-bonding pattern described above. Based on the behavior of the single mutants and analysis of molecular contacts, we made double mutants. R73A/N78A binds less well than R73A, and S77A/N78A binding is similar to that of S77A alone (Fig. 4*B*, Fig. S3 *A* and *C*, and Table 1). This result indicates a minor role for site A in the interaction of RAE1 with m152, an observation consistent with our evaluation of the contribution of the PLWY motif (residues 19–22) to m152 binding (21). For binding site B, where charge interactions seem to dominate the interface, we made five single mutants, Q151I, K154A, Y155A, E159A, and E159W. All these substitutions had a major effect on interaction with m152 (Fig. 4*B*, Table 1, and Fig. S3 *A* and *C*). We then tested the binding affinity of four additional double mutants of RAE1γ (R73A/K154A, K154A/Y155A, K154A/E159A, and E159A/R161A) and one triple mutant (K154A/Y155A/E159A). E159A/R161A ($\Delta\Delta G$ =1.88 kcal/mol) binds more weakly than wild type, and R73A/K154A, K154A/Y155A, K154A/E159A, and K154A/Y155A/E159A all interacted very weakly with m152 (Fig. 4*B*, Table 1, and Fig. S3 *A* and *C*). The analysis of these mutants at both sites supports a general view that the interface is broad and redundant, an interpretation consistent with the relatively small impact of the site A mutants that we have examined.

Another way to confirm the site of interaction of m152 with RAE1 is to consider the differential affinity of the RAE1 isoforms, which differ in the regions of the site A and B contacts (Figs. S2*A* and S4). To compare these differences, we determined the binding affinity of RAE1 isoforms β, γ, δ, and ε by surface plasmon resonance (SPR) (Fig. 4*B* and Fig. S3 *B* and *C*). RAE1β binds to

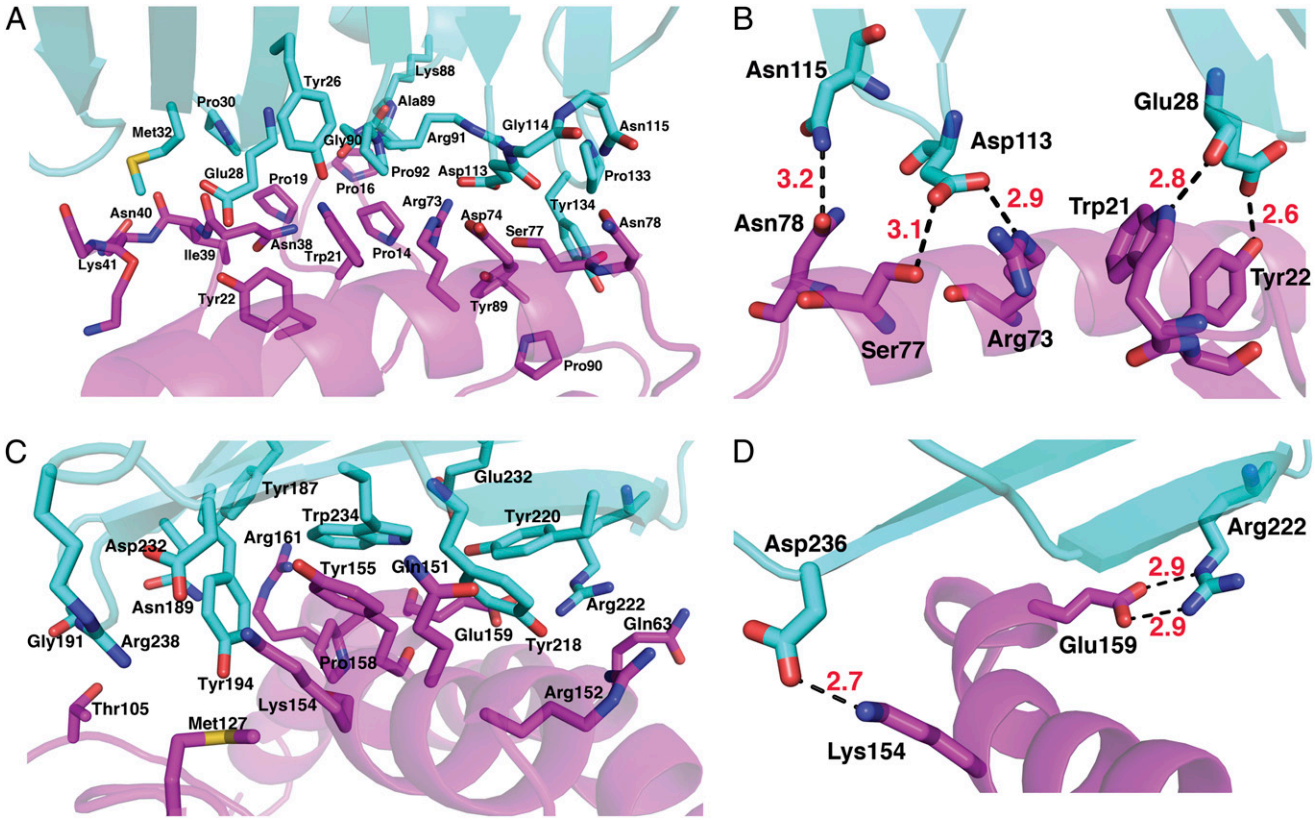

Fig. 3. Interaction between m152 and RAE1γ. (*A*) The major contact residues at site A. (*B*) Hydrogen bonds at site A. (*C*) Contacts at site B. (*D*) Hydrogen bonds at site B. m152 and RAE1γ are cyan and magenta, respectively. Nitrogen, oxygen, and sulfur atoms are colored blue, red, and yellow, respectively. Hydrogen bonds (distance <3.2 Å) are shown as dashed black lines, and distances are labeled.

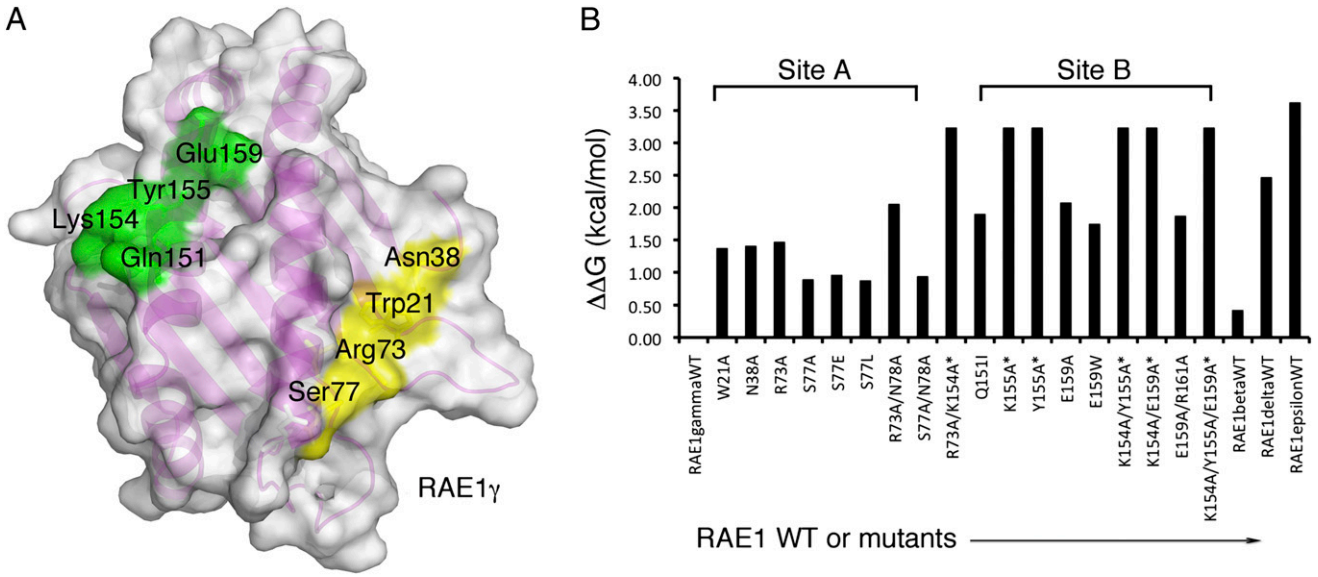

Fig. 4. Mutational analysis confirms RAE1γ hotspots. (*A*) A surface representation of the interacting surface of RAE1γ is shown. The positions of mutants that cause the greatest effect on binding are colored yellow ($\Delta\Delta G$ = 0.8–1.5 kcal/mol) and green ($\Delta\Delta G$ >1.5 kcal/mol). (*B*) Summary of $\Delta\Delta G$ for all mutants tested. An asterisk indicates that K_d was >100 μM.

m152 with a K_d about 0.86 μM, and RAE1γ binds slightly more strongly (K_d 0.42 μM). RAE1δ binds to m152 less well (K_d = 27.4 μM), and RAE1ε binds with the weakest affinity (K_d = 193 μM). These values indicate somewhat higher affinities than those we reported for RAE1β, RAE1γ, and RAE1δ, based on analytical ultracentrifugation studies (21) but are in the same rank order, and we extend these measurements to the ε isoform. Comparisons of the X-ray structures of RAE1β [Protein Data Bank (PDB) ID 1JFM] and RAE1γ (taken from the complex reported here; PDB ID 4G59) and of molecular models of RAE1α, RAE1δ, and RAE1ε based on RAE1γ suggest a structural explanation for the similarities and differences observed in the binding of these isoforms to m152. RAE1γ, RAE1β, and RAE1α all conserve the PLWY motif (residues 19–22) and the K154/E159 motif im-

Table 1. Summary of affinity of the interactions of RAE1γ mutants to m152, mNKG2D, and anti-RAE1 antibody

	m152–surface		mNKG2D–surface		anti-RAE1–surface	
RAE1γ	K_d (μM)	$\Delta\Delta G$ (kcal/mol)	K_d (μM)	$\Delta\Delta G$ (kcal/mol)	K_d (μM)	$\Delta\Delta G$ (kcal/mol)
Wild type	0.42	0.00	0.43	0.00	5.54	0.00
Binding site A mutants						
W21A	4.30	1.38	1.63	0.79	5.79	0.02
N38A	4.56	1.41	4.19	1.35	6.36	0.08
R73A	5.07	1.47	1.15	0.59	1.58	−0.75
S77A	1.90	0.89	0.11	−0.80	4.06	−0.19
S77E	2.13	0.96	0.38	−0.07	4.08	−0.18
S77L	1.85	0.88	0.83	0.39	5.51	−0.01
R73A/N78A	13.50	2.06	3.50	1.25	4.71	−0.10
S77A/N78A	2.07	0.94	0.49	0.08	1.01	−1.01
Binding site B mutants						
R73A/K154A	>100	>3.24	>100	>3.23	6.17	0.06
Q151I	10.50	1.91	1.47	0.73	6.18	0.06
K154A	>100	>3.24	12.50	2.00	6.99	0.13
Y155A	>100	>3.24	29.50	2.51	4.21	−0.17
E159A	14.10	2.08	15.00	2.11	7.78	0.20
E159W	8.10	1.75	18.80	2.24	6.06	0.05
K154A/Y155A	>100	>3.24	>100	>3.23	7.18	0.15
K154A/E159A	>100	>3.24	>100	>3.23	5.57	0.00
E159A/R161A	10.00	1.88	15.80	2.14	6.28	0.07
K154A/Y155A/E159A	>100	>3.24	>100	>3.23	6.43	0.08

Binding of wild-type and mutant RAE1γ molecules was measured by SPR as described in *Materials and Methods*. K_d was determined and $\Delta\Delta G$ values were calculated according to the relationships $\Delta G = RT\ ln\ K_d$, $R = 1.986 \times 10^{-3}$ kcal/(K*mol), T = 298 K, and $\Delta\Delta G = \Delta G_{mutant} - \Delta G_{wt}$. Curves showing little or no binding were estimated to have K_d of >100 μM as indicated, and the resulting calculated $\Delta\Delta G$ values are minimal estimates.

portant for m152 binding. RAE1δ has deleted the PLWY motif (which contributes to binding significantly via W21) and also has lost the residue equivalent to E159 (G155 in RAE1δ), accounting for its lower affinity. RAE1ε, in addition to a rearrangement of the PLWY motif, has a deletion of residues 56 and 57 at the beginning of the α1 helix and also has substituted the important E159 with Q (i.e., Q157). The drastic cumulative effect of the 56–57 deletion and the Q157 substitution is evident in the appearance of a large basic patch at the N-terminal part of the α1 helix and the C-terminal part of the α2 helix (Fig. S4).

m152 Differentially Down-Regulates Surface Expression of RAE1γ and Mutants in Transfected HEK293T Cells. The recognized biological function of m152 is to bind RAE1 or MHC-I molecules in the endoplasmic reticulum-*cis* Golgi compartment (ERGIC) (18), thus impeding the rate of their maturation and appearance at the cell surface. One would expect that low-affinity RAE1 isoforms or mutants that impair the interaction with m152 would be down-regulated less efficiently when coexpressed with m152. To test the effects of RAE1γ mutations, we cotransfected wild-type RAE1γ and site-directed mutants with wild-type m152 in a GFP vector into HEK293T cells and measured the cell-surface expression of RAE1γ by cytofluorimetry. As shown in Fig. 5, cells cotransfected with RAE1γ and an empty GFP vector express large amounts of RAE1 on the cell surface in 95% of the GFP^+ cells. Transfection with the same vector harboring full-length m152 significantly prevents the cell-surface expression of RAE1, so that only 11% of the GFP^+ cells are also $RAE1^+$. When cells are transfected with the S77A RAE1γ mutant that retains a high affinity for m152, RAE1 surface expression also is down-regulated efficiently, with only 13% of GFP^+ cells being $RAE1^+$. In contrast, the double and triple mutants K154A/Y155A and K154A/Y155A/E159A, which show no measureable binding to either m152 or NKG2D (Table 1 and Figs. *S3A* and S5), are significantly less well down-regulated by m152. They express RAE1 at the surface on 91% and 94% of the GFP^+ transfectants. Thus, the cell-surface down-regulation of transfected RAE1γ by m152 is hampered significantly by multiple mutations at the site B interface.

Comparison with the NKG2D/RAE1β Complex. Having confirmed the m152/RAE1γ interface by site-directed mutagenesis, we then compared the m152/RAE1γ structure with known structures of the mNKG2D/RAE1β (11), hNKG2D/ULBP3 (12), and hNKG2D/MICA (32) complexes (Fig. 6 *A–E*). The structure of mNKG2D/RAE1β reveals that the NKG2D monomer makes contacts with the α1 and α2 helices of the RAE1 pd (11). The total buried solvent-accessible surface area of the m152/RAE1γ interface (about 2,600 $Å^2$) is greater than the buried surface area of the mNKG2D/RAE1β (1,700 A^2), hNKG2D/ULBP3 (1,920 $Å^2$), and the hNKG2D/MICA (2,287 $Å^2$) interfaces. Binding analysis indicated that the m152/RAE1γ interaction (K_d 0.42 μM) is about the same as that of mNKG2D/RAE1γ (K_d 0.43 μM). NKG2D chain A interacts with RAE1β residues that are involved in site A (of RAE1γ) in the m152 complex, and NKG2D chain B interacts with many of the RAE1 residues of site B (Table S4). Many of the same residues of RAE1 are exploited in their contacts with either the NKG2D or m152 ligand.

Identification of RAE1 contact residues with m152 and NKG2D indicates that these two ligands should compete for binding to RAE1. Although the biological interaction of RAE1 with m152, both of which are expressed in the ERGIC of the host cell, is a *cis* interaction, and that of RAE1 with the NKG2D homodimer, is an extracellular *trans* interaction, it is instructive to evaluate the site of interaction in vitro by competition. Increasing concentrations of m152 with a fixed concentration (3 μM) of RAE1γ were offered to mNKG2D-Fc, and the binding response of mNKG2D to RAE1γ decreased (Fig. 6 *F* and *G*). We conclude that m152 and NKG2D bind the same site on RAE1γ. Further confirmation that these molecules bind the same site on RAE1 was obtained by direct analysis of the binding of RAE1γ mutants. Using SPR, we show that RAE1γ mutants that affect m152 binding also, by and large, affect NKG2D binding, but have little effect on binding to an anti-

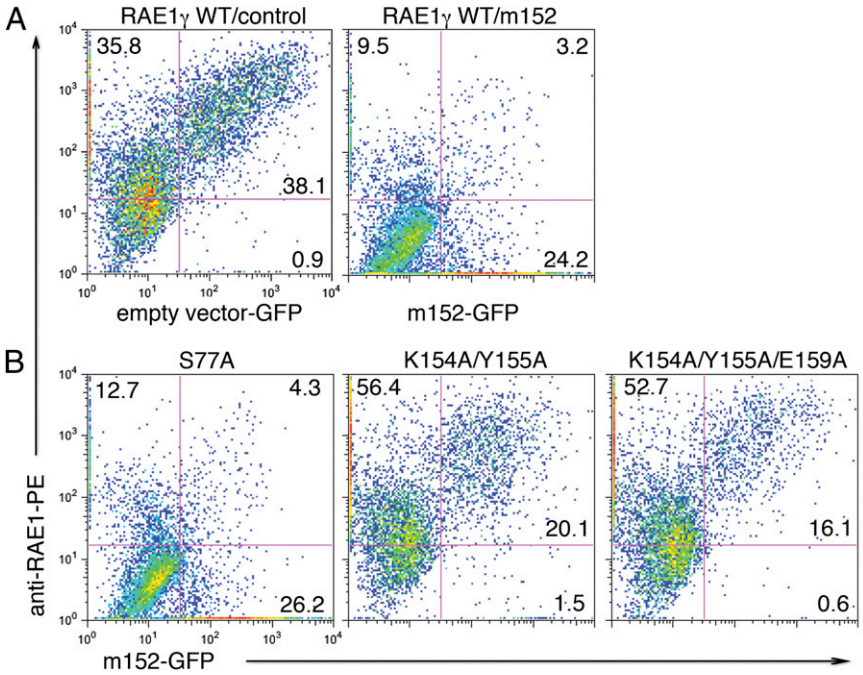

Fig. 5. m152 differentially down-regulates the surface expression of wild-type RAE1γ and interface mutants. (*A*) Expression of wild-type RAE1γ with empty vector carrying an IRES-GFP (*Left*) or m152 containing an IRES-GFP vector (*Right*). (*B*) Expression of RAE1γ mutants S77A (*Left*), K154A/Y155A (*Center*), and K154A/Y155A/E159A (*Right*). Cells were stained with mAb to RAE1 and analyzed by flow cytometry for surface expression of wild-type RAE1γ or mutants. Data are representative of three independent experiments with similar results.

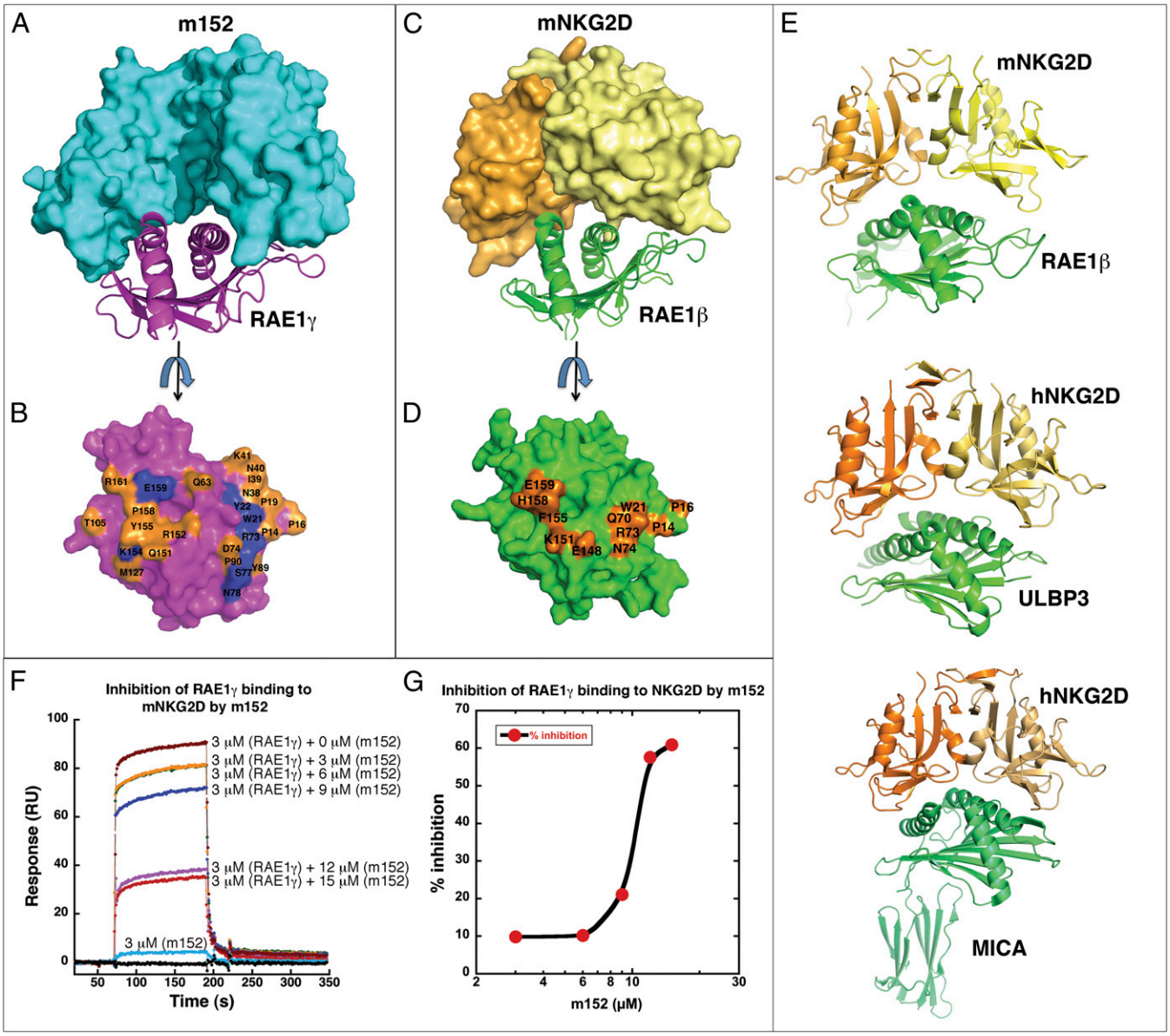

Fig. 6. m152 competes with mNKG2D for binding RAE1. (*A–D*) Comparison of surface interactions between m152 with RAE1γ (*A* and *B*) and between mNKG2D and RAE1β (*C* and *D*). (*A*) m152 (cyan) shown in a surface representation and RAE1γ (magenta) as ribbon. (*C*) mNKG2D homodimer (yellow and orange) in a surface representation and RAE1β (green) shown as ribbon. (*B* and *D*) Rotation about the *y* axis of ~90° from *A* and *C*, with RAE1γ (*B*) and RAE1β (*D*) shown in surface representation. The residues of RAE1γ (*B*) and RAE1β (*D*) contact m152 or mNKG2D. Contact sites are colored in orange and hydrogen bonds in blue. (*E*) Comparison of mNKG2D/RAE1β (PDB ID 1JSK), hNKG2D/ULBP3 (PDB ID 1KCG), and hNKG2D/MICA (PDB ID 1HYR) complexes. The structures were superposed and are shown as ribbons in the same orientation. (*F* and *G*) SPR binding analysis of the competitive binding in the m152:RAE1γ:mNKG2D interaction. (*F*) SPR-based study of competition between mNKG2D and m152 for binding RAE1γ. mNKG2D-Fc was captured over a CM5 biosensor chip. Fixed amounts of RAE1γ (3 μM) without or with increasing amount of m152 (3, 6, 9, 12, and 15 μM) were flowed over the immobilized mNKG2D-Fc surface. m152 alone (3 μM) was offered to the NKG2D-Fc surface as a negative control. (*G*) The data in *F* are plotted as percent inhibition.

RAE1 mAb (Figs. S3*A*, S5, and S6 and Table 1). These SPR results reveal that, despite the profound differences in the structures of m152 and mNKG2D, their binding sites on RAE1γ are remarkably similar. In particular, the α2 helix domain residues of RAE1γ, including Lys154, Tyr155, and Glu159, form an important contact site for both m152 and NKG2D.

Structure Comparison with Other CMV-Encoded Immunoevasin Complexes. The crystal structure of the m152/RAE1γ complex describes in detail an MCMV-encoded protein bound to its ligand and, more importantly, represents a complex of two MHC-I–like molecules—an MCMV immunoevasin and its MHC-I–like stress-induced ligand. Three complexes of HCMV-encoded molecules with their respective ligands have been reported: the complex of the Ig-like US2 with HLA-A2 (33), that of the MHC-I–like UL18 with the Ig-like LIR-1 (34), and that of the Ig-like UL16 with the MHC-I–like hNKG2D ligand MICB (29). In all these complexes, the viral molecule exploits a different aspect of the host cell's ligand for interaction. The Ig-like US2 binds HLA-A2 through a modestly sized interface involving the junction of the α1α2 pd with the α3 domain, and UL16 interacts strongly (through an interface of ~2,200 Å^2) with the α2 helix of MICB (Fig. S7 *A–D*). Superposition of the m152/RAE1γ structure with that of the UL16/MICB complex indicates that the Ig-like domains of both m152 and UL16 in-

terface with a similar patch on the α2 domain of RAE1γ or MICB, respectively. In contrast, the other MHC-I–like viral homolog, UL18, which binds to the host inhibitory receptor LIR-1 at the cell surface, makes contacts through its α3 domain and β2m subunits, a region reminiscent of the site of classical MHC-I molecules where CD8αα, CD8αβ, and murine NK receptors of the Ly49 family interact (Fig. S4).

Discussion

MCMV, like other large DNA viruses, employs many of its genes to counter the host's inflammatory and immune responses to infection. Our analysis of the structure, binding, and function of the MCMV m152 glycoprotein in its interaction with its host cell ligand RAE1γ shows that the MHC-I protein fold, apparently purloined from the host, has evolved to benefit the virus and also offers a snapshot of the ongoing mutual evolution by which the host counters viral infection and the virus then acquires new functions to resist the host's immunity. m152 is a unique molecule in that it not only down-regulates the expression of RAE1 receptors that are ligands for NKG2D but also limits the cell-surface expression of MHC-I molecules, which serve as targets of both NK inhibitory and T-cell receptors. The structure of the m152/RAE1γ complex sheds light on the specificity of m152/RAE1 interactions, as compared with the diverse ligand interactions of NKG2D, and offers a framework that allows us to model the interaction of m152 with host MHC-I and to speculate on the progressive evolution of the MCMV immunoevasins m145, m152, and m155 along with their respective ligands, MULT1, RAE1, and H60.

The *trans* interaction of mNKG2D with RAE1 (35) and H60 (36), which leads to NK cell activation, has been examined carefully quantitatively and, for RAE1, structurally as well (11). Detailed analysis of NKG2D interactions with its ligands of several different families has led to the conclusion that NKG2D interacts via rigid adaptation (35, 37), a mechanism whereby the initial interaction is via a "lock and key" mechanism, but for some ligands the stabilization of the interaction requires conformational adjustment of residues at the periphery of the interaction site. For the m152/RAE1 *cis* interaction, in the absence of a structure of unliganded m152 or RAE1γ, we cannot determine whether there is significant molecular adjustment of the m152.

The MHC-fold is characterized by the structure of the MHC-I α1α2 pd, formed by the homologous α1 and α2 domains that assemble in pseudosymmetrical rotational symmetry to form the peptide-binding site and the distinct Ig-like α3 domain. m152 is an MHC-I–like molecule, preserving the MHC pd and the C1-type Ig-fold for α3. It exploits each of these structural units to generate two distinct sites for interaction with RAE1. Given the localization of the interaction of m152 to sites A and B, where site A (of m152) is derived from the platform supporting the α1 and α2 helices and site B from the α3 domain, it is reasonable to speculate that m152 interacts with classical MHC-I using the same surfaces and general orientation. To illustrate this notion, we superposed the α1α2 domain of the MHC-I molecule H2-D^d on the α1α2 structure of RAE1γ as shown in Fig. S7*E*. This arrangement suggests that the solvent-accessible region between the two contact sites may provide space to accommodate some side chains of an MHC-I–bound peptide.

Aside from the interactions of the MCMV MHC-Iv molecules with their MHC-I–like NKG2D ligands, the only other known MHC/MHC interactions are those between the classical MHC-II molecule HLA-DR and HLA-DM (38) (H2-IA and H2-DM in the mouse) and between HLA-DO and HLA-DM (39). Although the structural details of these interactions have not yet been reported, efforts using mutagenesis, FRET, and molecular modeling (40, 41) suggest that a large lateral interface of DO with DM or of DM with DR is involved. This interface contrasts sharply with the interaction surface of m152, which exploits its α1α2 pd and its α3 Ig-like domains. MHC and MHC-like molecules thus can use different faces for interaction—the "top," including the α1 and α2 domain helices and bound peptide (for classical MHC-I), for interaction with TCR or KIR NK receptors; the "side," consisting of the junction of the α1α2 platform with α3, for interaction with US2 (Fig. S7*B*); or the "bottom," consisting of the underside surface of α1α2 along with the α3 domain, for interaction with CD8 and Ly49 receptors and in the interaction of m152 with RAE1γ (31, 42).

We also must consider the structure of the MCMV MHC-Iv molecules m145, m152, and m155, in view of their ongoing evolution to improve viral fitness in the face of host adaptation. Although these three proteins are only 11–15% identical in the amino acid sequences of their extracellular domains, they may be aligned sensibly when predictions regarding secondary structure are taken into account (19, 43). We speculate that the host stress response leading to expression of an NKG2D ligand was an early step in the coevolution of the host NKG2D ligands and the viral evasins. Analysis of the sequences of MULT1, H60, and RAE1 (Fig. S2*B*) (as well as those of MIC and ULBP in the human, and the MIC-related MILL of the mouse) indicates that these sequences derive from an ancestral prototype gene (44, 45) and that the three mouse families, H60, RAE1, and MULT1, can be categorized as clearly distinct clusters, not only by sequence and gene location but also by virtue of the GPI anchor of H60 and RAE1. Which of the existing murine NKG2D ligands was evolutionarily the earliest? MULT1 is more distant from the other two families, but comparative sequence analysis suggests the emergence of the MIC, MILL, and ULBP genes in the MHC in a common ancestor of marsupial and placental mammals (45). This analysis suggests that first the MILL genes and then the ULBP genes (of which the MULT1, RAE1, and H60 subfamilies are part) emigrated as well. Finally, the rodents lost the MIC genes, and humans lost MILL. Because these NKG2D ligands exist in multiple copies and have a high turnover rate (46), the consistent emergence of immunoevasins to deal with MULT1, RAE1, and H60 variation led to the evolution of m145, m152, and m155 as well as the non–MHC-Iv gene m138 in the mouse. Our structural studies firmly establish the MHC-I–like structure of m152, adding it to the solved structures of m144, m153, and m157, and explain the nature of its interaction with its RAE1 ligands. We expect that m145 binds MULT1 in a similar orientation and that m155 interacts with H60 in a like manner. The full story, however, must await the determination of the structure of each of these binary complexes and of each of these NKG2D ligands with NKG2D as well. A more speculative analysis is required for predicting the nature of the structural interaction of the HCMV MHC-Iv protein UL142 with its MICA stress-induced NKG2D ligand (47), because UL142, unlike MCMV immunoevasins, is a truncated MHC-Iv molecule lacking an α3 domain and because MICA, like MICB but unlike other human and murine NKG2D ligands, includes an α3 domain. Thus, we propose that the MICA/UL142 complex will mimic the m152/RAE1γ structure but with the partners reversed. The larger MICA would be expected to straddle the smaller UL142 in the ERGIC, localized there by the UL142 transmembrane domain. Although many pieces of the function, structure, and evolution of the CMV/MHC-Iv/immunoevasin puzzle remain unknown, we expect that additional components soon will be discovered and put in their appropriate places.

Materials and Methods

Expression and Purification of Soluble m152 and RAE1. Expression and purification of the ectodomain of m152 linked to a C-terminal His6 tag from *Drosophila* S2 cells and *Escherichia coli* expression of wild-type RAE1γ were described previously (21, 22). m152 expression was induced with 1 mM CuSO4 for 5 d. The supernatant was collected and was purified by chelate agarose chromatography followed by size-exclusion chromatography on a Superdex 75 16/60 prep grade column (GE Healthcare Life Science) and by ion exchange on a mono Q 5/50 GL column (GE Healthcare Life Science). Protein purity was confirmed by SDS/PAGE and by N-terminal sequencing.

We expressed four isoforms of the RAE1 ectodomain (β, γ, δ, and ε) from pET21b constructs in *E. coli* Rosetta 2(DE3) and refolded native proteins from inclusion bodies as described previously (21). Refolded proteins were purified by size-exclusion chromatography and were kept in 25 mM Tris, pH7.4, 50 mM NaCl. All RAE1 isoforms and mutants were expressed similarly. (Efforts to express and refold RAE1α by the same or similar protocols gave poor yields). Site-specific mutants were created with the QuikChange multisite-directed mutagenesis kit (Stratagene). All mutants were confirmed by DNA sequencing and purified following the protocol used for the wild-type protein.

Crystallization and Data Collection. m152 and RAE1γ were mixed in a 1:1 molar ratio (total concentration 1 mg/mL) for 1 h at 4 °C and then were loaded on a Shodex Protein KW-802.5 gel filtration column to obtain the m152/RAE1γ complex. This complex then was concentrated to 10 mg/mL in 50 mM Tris, pH 7.5, 50 mM NaCl and crystallized by hanging drop vapor diffusion at 18 °C. The crystal formed within 1 mo in 0.2 M KCl, 15% (wt/vol) PEG 3350. The single crystal was soaked in reservoir solution with 15% (vol/vol) ethylene glycol and then was flash-frozen in liquid nitrogen for data collection. X-ray diffraction data were collected at 100 K at beamline X29 at the National Synchrotron Light Source, Brookhaven Laboratories (Upton, NY), at a wavelength of 1.0 Å. Data to 2.45 Å were indexed, integrated, and scaled with HKL2000 (48). Data collection and refinement statistics are reported in Table S1.

Structure Determination, Refinement, and Structure Analysis. The crystal belongs to space group C2 and contains two complexes in the asymmetric unit. The structure was solved by molecular replacement in Phaser of the CCP4 suite (49), by using m153 (PDB ID 2O5N) and RAE1β (PDB ID 1JFM) as search models. After an initial round of rigid body refinement, the model was fitted manually with Coot (50) and then was refined with energy minimization, B factor refinement, and water addition using the CNS 1.3 program suite (51). Final refinement was carried out with Phenix (52). The final model has R_{free} = 24% and R_{factor} = 20% and includes residues 1–264 of m152 and residues 2–41 and 52–173 of RAE1γ. The electron density of the surface loop region (residues 42–51 of chain A, residues 43–51 of chain B) of RAE1γ was not visualized. Two N-linked glycosylation sites were identified at positions 61 and 208 of m152. Analysis of the final structure was performed with MolProbity (53) and PDBsum (54). All structural figures were created with PyMOL Molecular Graphics System, version 1.5.0.1 (Schrödinger, LLC, www.pymol.org). Coordinates and structure factors have been deposited with the Protein Data Bank (ID code 4G59).

SPR Binding Assays and Data Analysis. All SPR experiments were performed using a BIAcore2000 Biosensor (Biacore) at 25 °C in HBS-EP buffer (BIAcore). Purified recombinant m152 protein was immobilized on a research-grade CM5 chip (BIAcore) with standard 1-ethyl-3-(3-dimethylaminopropyl) carbodiimide/NHS coupling. Recombinant mouse NKG2D-Fc (catalog no. 139-NK) and mouse RAE1 pan-specific mAb (catalog no. MAB17582) were purchased from R&D Systems. One thousand response units (RU) of each protein were immobilized. After buffer exchange to HBS-EP, wild-type RAE1γ, mutants, and RAE1 isoforms (β, δ, and ε) were offered to the immobilized protein surface at 30 μL/min. All measurements were conducted over a range of concentrations of the solution phase analyte. After binding and washout, sensorgrams were monitored to assure return to baseline. No regeneration step was used. All measurements were made in at least two independent experiments. Data were analyzed with the surface site distribution model with EVILFIT (55) or with by BIAevaluation 3.0 (GE Healthcare Life Sciences). For competition experiments, 1,000 RU of recombinant mouse NKG2D-Fc was immobilized on a CM5 chip (BIAcore), and wild-type RAE1γ with or without additional m152, was offered to the immobilized mNKG2D-Fc surface.

Transfection and flow cytometry. HEK293T cells were grown in complete RPMI medium. Transient transfection of HEK293T cells was performed with Fugene6 (Roche) according to the manufacturer's instruction. The N-terminally FLAG-tagged full-length m152 gene (including the signal peptide sequence) was cloned into pIRES-hr-GFP-II (Agilent Technologies), and full-length wild-type RAE1γ and RAE1γ S77A, K154A/Y155A, or K154A/Y155A/E159A mutant cDNAs were each cloned into pcDNA3.1. Then 0.5 μg of either m152-pIRES-hr-GFPII or empty pIRES-hr-GFPII was mixed with 0.5 μg of the RAE1γ construct. The mixture was added to Fugene6 for transfection of HEK293T and was maintained at 37 °C, 5% CO_2. At 48 h, cells were harvested, washed with FACS buffer (PBS, 2% FCS, 0.05% NaN3). Cells were stained with phycoerythrin-labeled mouse anti-RAE1 mAb 186107 (R&D Systems), washed three times, and analyzed on a FACSalibur (Becton Dickinson) using FlowJo (Treestar).

ACKNOWLEDGMENTS. We thank Xavier Ambroggio and Michael Dolan for help with docking programs. This research was supported by the intramural research program of the National Institute of Allergy and Infectious Diseases, National Institutes of Health.

1. Reddehase MJ (2002) Antigens and immunoevasins: Opponents in cytomegalovirus immune surveillance. *Nat Rev Immunol* 2(11):831–844.
2. Sissons JG, Carmichael AJ, McKinney N, Sinclair JH, Wills MR (2002) Human cytomegalovirus and immunopathology. *Springer Semin Immunopathol* 24(2):169–185.
3. Lenac T, Arapović J, Traven L, Krmpotić A, Jonjić S (2008) Murine cytomegalovirus regulation of NKG2D ligands. *Med Microbiol Immunol (Berl)* 197(2):159–166.
4. Lanier LL (2008) Evolutionary struggles between NK cells and viruses. *Nat Rev Immunol* 8(4):259–268.
5. Jonjić S, Babić M, Polić B, Krmpotić A (2008) Immune evasion of natural killer cells by viruses. *Curr Opin Immunol* 20(1):30–38.
6. de Kruijf EM, et al. (2012) NKG2D ligand tumor expression and association with clinical outcome in early breast cancer patients: An observational study. *BMC Cancer* 12:24.
7. McGilvray RW, et al. (2010) ULBP2 and RAET1E NKG2D ligands are independent predictors of poor prognosis in ovarian cancer patients. *International Journal of Cancer* 127(6):1412–1420.
8. Cerwenka A, et al. (2000) Retinoic acid early inducible genes define a ligand family for the activating NKG2D receptor in mice. *Immunity* 12(6):721–727.
9. Carayannopoulos LN, Naidenko OV, Fremont DH, Yokoyama WM (2002) Cutting edge: Murine UL16-binding protein-like transcript 1: A newly described transcript encoding a high-affinity ligand for murine NKG2D. *J Immunol* 169(8):4079–4083.
10. Diefenbach A, Jamieson AM, Liu SD, Shastri N, Raulet DH (2000) Ligands for the murine NKG2D receptor: Expression by tumor cells and activation of NK cells and macrophages. *Nat Immunol* 1(2):119–126.
11. Li P, McDermott G, Strong RK (2002) Crystal structures of RAE-1beta and its complex with the activating immunoreceptor NKG2D. *Immunity* 16(1):77–86.
12. Radaev S, Rostro B, Brooks AG, Colonna M, Sun PD (2001) Conformational plasticity revealed by the cocrystal structure of NKG2D and its class I MHC-like ligand ULBP3. *Immunity* 15(6):1039–1049.
13. Lodoen M, et al. (2003) NKG2D-mediated natural killer cell protection against cytomegalovirus is impaired by viral gp40 modulation of retinoic acid early inducible 1 gene molecules. *J Exp Med* 197(10):1245–1253.
14. Krmpotic A, et al. (2005) NK cell activation through the NKG2D ligand MULT-1 is selectively prevented by the glycoprotein encoded by mouse cytomegalovirus gene m145. *J Exp Med* 201(2):211–220.
15. Lodoen MB, et al. (2004) The cytomegalovirus m155 gene product subverts natural killer cell antiviral protection by disruption of H60-NKG2D interactions. *J Exp Med* 200 (8):1075–1081.
16. Krmpotić A, et al. (2002) MCMV glycoprotein gp40 confers virus resistance to CD8+ T cells and NK cells in vivo. *Nat Immunol* 3(6):529–535.
17. del Val M, et al. (1992) Cytomegalovirus prevents antigen presentation by blocking the transport of peptide-loaded major histocompatibility complex class I molecules into the medial-Golgi compartment. *J Exp Med* 176(3):729–738.
18. Ziegler H, et al. (1997) A mouse cytomegalovirus glycoprotein retains MHC class I complexes in the ERGIC/cis-Golgi compartments. *Immunity* 6(1):57–66.
19. Mans J, et al. (2009) Structure and function of murine cytomegalovirus MHC-I-like molecules: How the virus turned the host defense to its advantage. *Immunol Res* 43(1-3): 264–279.
20. Arapović J, Lenac Rovis T, Reddy AB, Krmpotić A, Jonjić S (2009) Promiscuity of MCMV immunoevasin of NKG2D: m138/fcr-1 down-modulates RAE-1epsilon in addition to MULT-1 and H60. *Mol Immunol* 47(1):114–122.
21. Zhi L, et al. (2010) Direct interaction of the mouse cytomegalovirus m152/gp40 immunoevasin with RAE-1 isoforms. *Biochemistry* 49(11):2443–2453.
22. Mans J, et al. (2007) Cellular expression and crystal structure of the murine cytomegalovirus major histocompatibility complex class I-like glycoprotein, m153. *J Biol Chem* 282(48):35247–35258.
23. Holm L, Rosenstrom P (2010) Dali server: Conservation mapping in 3D. *Nucleic Acids Research* 38(Web Server issue):W545–549.
24. Halaby DM, Poupon A, Mornon J (1999) The immunoglobulin fold family: Sequence analysis and 3D structure comparisons. *Protein Eng* 12(7):563–571.
25. Adams EJ, et al. (2007) Structural elucidation of the m157 mouse cytomegalovirus ligand for Ly49 natural killer cell receptors. *Proc Natl Acad Sci USA* 104(24): 10128–10133.
26. Natarajan K, et al. (2006) Crystal structure of the murine cytomegalovirus MHC-I homolog m144. *J Mol Biol* 358(1):157–171.
27. Rudolph MG, Stanfield RL, Wilson IA (2006) How TCRs bind MHCs, peptides, and coreceptors. *Annu Rev Immunol* 24:419–466.
28. Steinle A, et al. (2001) Interactions of human NKG2D with its ligands MICA, MICB, and homologs of the mouse RAE-1 protein family. *Immunogenetics* 53(4):279–287.
29. Müller S, Zocher G, Steinle A, Stehle T (2010) Structure of the HCMV UL16-MICB complex elucidates select binding of a viral immunoevasin to diverse NKG2D ligands. *PLoS Pathog* 6(1):e1000723.
30. Radaev S, Sun PD (2003) Structure and function of natural killer cell surface receptors. *Annu Rev Biophys Biomol Struct* 32:93–114.

31. Wang J, et al. (2002) Binding of the natural killer cell inhibitory receptor Ly49A to its major histocompatibility complex class I ligand. Crucial contacts include both H-2Dd AND beta 2-microglobulin. *J Biol Chem* 277(2):1433–1442.
32. Li P, et al. (2001) Complex structure of the activating immunoreceptor NKG2D and its MHC class I-like ligand MICA. *Nat Immunol* 2(5):443–451.
33. Gewurz BE, et al. (2001) Antigen presentation subverted: Structure of the human cytomegalovirus protein US2 bound to the class I molecule HLA-A2. *Proc Natl Acad Sci USA* 98(12):6794–6799.
34. Yang Z, Bjorkman PJ (2008) Structure of UL18, a peptide-binding viral MHC mimic, bound to a host inhibitory receptor. *Proc Natl Acad Sci USA* 105(29):10095–10100.
35. McFarland BJ, Strong RK (2003) Thermodynamic analysis of degenerate recognition by the NKG2D immunoreceptor: Not induced fit but rigid adaptation. *Immunity* 19(6): 803–812.
36. O'Callaghan CA, Cerwenka A, Willcox BE, Lanier LL, Bjorkman PJ (2001) Molecular competition for NKG2D: H60 and RAE1 compete unequally for NKG2D with dominance of H60. *Immunity* 15(2):201–211.
37. Margulies DH (2003) Molecular interactions: Stiff or floppy (or somewhere in between?). *Immunity* 19(6):772–774.
38. Sloan VS, et al. (1995) Mediation by HLA-DM of dissociation of peptides from HLA-DR. *Nature* 375(6534):802–806.
39. Liljedahl M, et al. (1996) HLA-DO is a lysosomal resident which requires association with HLA-DM for efficient intracellular transport. *EMBO J* 15(18):4817–4824.
40. Yoon T, et al. (2012) Mapping the HLA-DO/HLA-DM complex by FRET and mutagenesis. *Proc Natl Acad Sci USA* 109(28):11276–11281.
41. Zwart W, et al. (2005) Spatial separation of HLA-DM/HLA-DR interactions within MIIC and phagosome-induced immune escape. *Immunity* 22(2):221–233.
42. Wang R, Natarajan K, Margulies DH (2009) Structural basis of the CD8 alpha beta/ MHC class I interaction: Focused recognition orients CD8 beta to a T cell proximal position. *J Immunol* 183(4):2554–2564.
43. Revilleza MJ, et al. (2011) How the virus outsmarts the host: Function and structure of cytomegalovirus MHC-I-like molecules in the evasion of natural killer cell surveillance. *J Biomed Biotechnol* 2011:724607.
44. Samarakoon A, Chu H, Malarkannan S (2009) Murine NKG2D ligands: "Double, double toil and trouble". *Mol Immunol* 46(6):1011–1019.
45. Kondo M, et al. (2010) Comparative genomic analysis of mammalian NKG2D ligand family genes provides insights into their origin and evolution. *Immunogenetics* 62(7): 441–450.
46. Eagle RA, Traherne JA, Ashiru O, Wills MR, Trowsdale J (2006) Regulation of NKG2D ligand gene expression. *Hum Immunol* 67(3):159–169.
47. Chalupny NJ, Rein-Weston A, Dosch S, Cosman D (2006) Down-regulation of the NKG2D ligand MICA by the human cytomegalovirus glycoprotein UL142. *Biochem Biophys Res Commun* 346(1):175–181.
48. Otwinowski Z, Minor W (1997) Processing of X-ray diffraction data collected in oscillation mode. *Methods in Enzymology*Carter CW, Jr, Sweet RM (Academic, New York), Vol 276: Macromolecular Crystallography, part A, pp 307–326.
49. Collaborative Computational Project, Number 4 (1994) The CCP4 suite: Programs for protein crystallography. *Acta Crystallogr D Biol Crystallogr* 50(Pt 5):760–763.
50. Emsley P, Cowtan K (2004) Coot: Model-building tools for molecular graphics. *Acta Crystallographica. Section D, Biological Crystallography* 60(Pt 12 Pt 1):2126–2132.
51. Brunger AT (2007) Version 1.2 of the Crystallography and NMR system. *Nat Protoc* 2 (11):2728–2733.
52. Adams PD, et al. (2010) PHENIX: A comprehensive Python-based system for macromolecular structure solution. *Acta Crystallogr D Biol Crystallogr* 66(Pt 2):213–221.
53. Chen VB, et al. (2010) MolProbity: All-atom structure validation for macromolecular crystallography. *Acta Crystallogr D Biol Crystallogr* 66(Pt 1):12–21.
54. Laskowski RA, et al. (1997) PDBsum: A Web-based database of summaries and analyses of all PDB structures. *Trends Biochem Sci* 22(12):488–490.
55. Svitel J, Balbo A, Mariuzza RA, Gonzales NR, Schuck P (2003) Combined affinity and rate constant distributions of ligand populations from experimental surface binding kinetics and equilibria. *Biophys J* 84(6):4062–4077.